Improving the experimental estimation of the incident angle modifier of evacuated tube solar collectors with heat pipes

J. M. Rodríguez-Muñoz[a,*], I. Bove[b], R. Alonso-Suárez[a,b]

[a] *Laboratorio de Energía Solar, Departamento de Física del Litoral, CENUR Litoral Norte, Universidad de la República*
[b] *Laboratorio de Energía Solar, Instituto de Física, Facultad de Ingeniería, Universidad de la República*

Abstract

This article focuses on the thermal performance testing of evacuated tube solar collectors with heat pipes (ETC-HP) using the ISO 9806:2017 standard test methods: Steady-state testing (SST) and Quasi-dynamic testing (QDT). The main objective of this work is to improve the experimental estimation of the incident angle modifier (IAM) for these types of solar collectors in both test methods. For the QDT method, a novel model for the IAM is presented and validated against SST results. This IAM model, recently developed for flat plate collectors under the SST framework, has demonstrated superior performance compared to other available models. This study marks its first application to ETC-HP technology, showcasing its adaptability across different technologies and test methods. While this work primarily focuses on ETC-HP collectors, the results are applicable to evacuated tubes in general. Thus, the generality of this model and its consistency with the SST method make it suitable for implementation in test standards as a general-purpose model. Regarding the SST method, and aiming to enhance consistency between testing methods, an improved parameter conversion from SST to QDT is also proposed, reducing IAM differences between test methods by 1 to 19 percentage points, with greater improvement at higher incidence angles.

Keywords: Solar thermal collector, incident angle modifier, evacuated tube, ISO 9806 standard.

1. Introduction

Solar thermal systems are used for a variety of applications including domestic hot water, heating and cooling of buildings, heat generation for industrial processes and electricity generation. Solar thermal collectors are the main component of these systems, capturing solar energy and transferring it to a working fluid; therefore, the thermodynamic characterisation of these devices is very important. This characterisation is usually carried out by means of standardised tests, being the ISO-9806 (2017) standard one of the most widely used in the world. Although there are other standards (ASHRAE-93, 2014; EN-12975, 2022), they all present a high degree of similarity, reason why they can be considered equivalent to each other (Rojas et al.,

*Corresp. author: J. M. Rodríguez-Muñoz, jrodrigue@fing.edu.uy

List of Symbols

$\dot{Q}_u$	Useful power produced by the collector, W.
$\eta_{0,b}$	Collector peak efficiency referred to direct solar irradiance.
$\eta_{0,hem}$	Collector peak efficiency referred to global solar irradiance.
θ	Incidence angle.
θ_L	Longitudinal angle of incidence.
θ_T	Transversal angle of incidence.
ϑ_a	Ambient air temperature, °C.
ϑ_i	Collector inlet temperature, °C.
ϑ_m	Mean temperature of heat transfer fluid, °C.
ϑ_o	Collector outlet temperature, °C.
a_1	Heat loss coefficient, $\mathrm{W/m^2K}$.
a_2	Temperature dependence of the heat loss coefficient, $\mathrm{W/m^2K^2}$.
a_5	Effective thermal capacity, $\mathrm{J/Km^2}$.
A_G	Gross area of collector, $\mathrm{m^2}$.
f_d	Diffuse fraction, G_{dt}/G_t.
G_{bt}	Direct solar irradiance on collector plane, $\mathrm{Wm^{-2}}$.
G_{dt}	Diffuse solar irradiance on collector plane, $\mathrm{Wm^{-2}}$.
G_t	Global solar irradiance on collector plane, $\mathrm{Wm^{-2}}$.
K_b	Incidence angle modifier for direct solar irradiance.
K_d	Incidence angle modifier for diffuse solar irradiance.
K_{bL}	Incidence angle modifier in the longitudinal plane.
K_{bT}	Incidence angle modifier in the transversal plane.
K_{hem}	Incidence angle modifier for global solar irradiance.
q	Volumetric flow rate, $\mathrm{L\,min^{-1}}$.
u	Surrounding air speed, $\mathrm{m\,s^{-1}}$.

2008). In fact, the latest version of the (EN-12975, 2022) standard has become a requirements standard from now on, referring to ISO-9806 (2017).

The ISO-9806 (2017) standard was initially developed for flat plate collectors and uncovered collectors. It was later extended to other low temperature collector technologies, such as evacuated tube collectors, then to medium and high temperature collectors; parabolic trough concentrators and Fresnel-type concentrators (Fischer et al., 2006; Janotte et al., 2009; Hofer et al., 2015). The ability of this standard to adapt to different technologies is one of its main strengths. In this sense, the standard proposes a generic thermodynamic model, adaptable according to the technology, which makes it possible to predict the useful power produced by a collector under different meteorological and usage conditions. This model has a set of characteristic parameters that must be determined experimentally for each collector. To determine them, the standard proposes two methods: the first one in steady state conditions (SST - Steady State Testing) and the second one in quasi-dynamic conditions (QDT - Quasy-Dynamic Testing). The thermodynamic model used in each case is slightly different, mostly related to the treatment of diffuse solar irradiance. However, the standard provides a procedure for converting the parameters from one model to another.

The SST method was the first to be developed and is still the most widely used. However, its implementation requires strict clear sky conditions to achieve steady state, which is a limitation for outdoor laboratories in climates with variable cloud cover. This limitation motivated the development of the second method, QDT, which requires the test to be performed under varying cloud conditions. The QDT is then more flexible than the SST in terms of variability requirements and incorporates transient phenomena and diffuse solar irradiance modelling. This methodology is widely accepted worldwide and has been adopted by laboratories in Europe (Fischer et al., 2004; García de Jalón et al., 2011; Osório & Carvalho, 2014; Zambolin & Del Col, 2012), the United States (Rojas et al., 2008) and Latin America (Kratzenberg et al., 2006; Rodríguez-Muñoz et al., 2020). Many of these works show compatibility with the SST methodology. The advantage of the QDT method over the SST is the number of annual tests that can be obtained under outdoor conditions in variable cloud cover weather. In particular, in a previous study (Rodríguez-Muñoz et al., 2020), we evaluated the applicability of this methodology for a flat-plate collector in the Pampa Húmeda region of South America (SESA, Southeastern South America). This analysis showed that the QDT methodology can achieve more than twice as many annual tests as the SST methodology in this region.

However, the QDT method has some drawbacks. For example, results vary depending on the averaging time used for the experimental data. Furthermore, some difficulties have been reported when trying to extend this methodology to evacuated tube collectors with heat pipes (QAiST, 2012; Osório & Carvalho, 2014). This type of collector has a very large time constant compared to other technologies, such as flat plate collectors, and the QDT method has difficulty in describing the temperature variations at the collector outlet. This makes it difficult to determine some characteristic parameters of evacuated tube collectors, particularly those related to the angle of incidence modifier. Although this topic has been studied and there are specific experimental guidelines for determining the IAM for this type of collector (QAiST, 2012), the implementation of QDT tests and the accurate determination of the IAM remains a challenge. In this sense, the nonlinearity of the IAM in these types of collectors makes the problem even more complicated. Furthermore, some discrepancies have been reported between the angle of incidence modifier for diffuse solar irradiance obtained by one methodology and another (Kovács et al., 2011), suggesting that the modelling of this parameter and the conversion of SST to QDT parameters can be improved.

In response to the above problems, several alternatives have been proposed. On the one hand, improved transient test methods have been developed (Kong et al., 2012, 2015; Xu et al., 2012, 2013; Hofer et al., 2015). These methods address some of the drawbacks of the traditional QDT method and, in particular, improve the modeling of the transient behavior of solar collectors. Nevertheless, these studies have focused on the application of these methods to a specific type of collector, and the extension of these techniques to ETC-HP collectors remains an open task. On the other hand, specifically regarding the determination of the IAM, several models for ETC collectors have been proposed within the framework of the traditional QDT method (Souka & Safwat, 1966; Sallaberry et al., 2011; Zambolin & Del Col, 2012; Osório & Carvalho, 2014). These models improve the IAM modeling for this type of collector while retaining the advantages of the traditional QDT method, such as its applicability to a wide range of technologies. While all of the aforementioned proposals are valuable, none of them stand out significantly in terms of performance. It is noteworthy that while the test standard proposes an IAM model for collectors with uniaxial IAM, known as the Ambrosetti function, no proposal is made for collectors with biaxial IAM, such as ETC collectors.

Finally, it is important to note that the ISO-9806 (2017) standard is currently under review. This review period offers a valuable opportunity to propose potential improvements and solutions to the aforementioned problems, including those suggested in this article, which are detailed in the following section.

1.1. Article's contribution

This work improves the experimental estimation of the IAM of ETC-HP technology, proposing modifications in both SST and QDT methods, which are described as follows.

For the QDT method, a novel model for IAM is presented and validated against the SST results. This IAM model was recently developed for flat plate collectors under the SST framework (Rodríguez-Muñoz et al., 2021b) and demonstrated superior performance compared to other available models (Souka & Safwat, 1966; Perers, 1997; Kalogirou, 2004). The present study represents its extension to the ETC-HP technology, demonstrating its applicability across different technologies and test methods, particularly in adapting to the more complex geometry of evacuated tubes, i.e., biaxial IAM. While this work focuses on ETC-HP collectors, the results can be extrapolated to evacuated tubes in general. In this sense, the generality of this model and its consistency with the SST method make it suitable for implementation in test standards as a general purpose model. In addition, the effect of using different averaging times on the experimental data is analysed and the most appropriate value for this variable is determined by comparison with results obtained using the SST method. This optimisation improves the accuracy of the IAM as well as the other characteristic parameters.

On the other hand, regarding the SST method, an enhanced parameter conversion procedure from SST to QDT is proposed. This method incorporates the diffuse fraction into the standard procedure, providing enhanced results for the IAM of the SST method and improving the compatibility between testing methodologies. All these previous analyses, including QDT and SST method, are demonstrated experimentally using the test data of two solar collectors of this type (ETC-HP).

Finally, this work provides some complementary contributions to the field. It identifies overlooked challenges in extending the QDT method to ETC-HP technology, attributed to its slow thermal response. In this respect, the data acquisition procedure of the QDT method for this type of collector and its subsequent processing are described in detail and guidelines are provided to improve the reliability of the results, complementing existing work in this field (QAiST, 2012). Furthermore, a free and documented parameter identification software is provided, using a constrained nonlinear regression algorithm. Currently, there are no freely available implementations of the QDT test, regardless of its optimisation methodology (linear or nonlinear). This availability not only provides a tool for testing laboratories, but also improves the reproducibility and validation of scientific work in the field. It is emphasized that this software is intended for general use with low-temperature glazed solar collectors, including both flat plate and evacuated tube technologies, that is, collectors with both uniaxial and biaxial IAM.

1.2. Article's outline

This article is organised as follows. In the following section, Section 2, the thermodynamic model of the ISO-9806 (2017) standard for low-temperature covered solar collectors is briefly described, along with the new IAM model for the QDT method. The test procedure and parameter identification algorithm are also described in this section. While the description covers both methods, it places particular emphasis on the QDT method and provides guidelines to improve the reliability of the results. Section 3 describes the test platform, the collectors tested and the measurements. Section 4 presents the results of both methods, including an analysis of the averaging time for the QDT method, and introduces the novel parameter conversion procedure (SST to QDT). Finally, Section 5 summarises the main conclusions of the work.

2. Methodology

This section describes the thermodynamic model used for each test method, including the novel IAM model for the QDT method, and the standard parameter conversion from SST to QDT model. Additionally, it includes a detailed description of the test procedure and the parameter identification algorithm for the QDT method.

2.1. QDT model and parameters

As mentioned in the introduction, the thermodynamics considered by the quasi-dynamic method of the ISO-9806 (2017) standard has a wide application and can be applied to different technologies of thermal solar collectors. The standard provides criteria on how to use the model for each case, specifying which terms can be omitted in the general equation depending on the solar collector technology. The suggested model for low-temperature collectors with cover is shown in Eq. (1),

$$\frac{\dot{Q}_u}{A_G} = \eta_{0,b} \left[K_b \left(\theta \right) \; G_{bt} + K_d \; G_{dt} \right] - a_1 \left(\vartheta_m - \vartheta_a \right) - a_2 \left(\vartheta_m - \vartheta_a \right)^2 - a_5 \frac{d\vartheta_m}{dt}, \tag{1}$$

where $\dot{Q}_u$ is the useful power produced by the collector, G_{bt} and G_{dt} are the direct and diffuse solar irradiance on the collector plane, respectively, ϑ_m the average temperature of the fluid passing through the collector (average between the inlet and outlet temperatures), ϑ_a the ambient temperature, and the parameters that characterize the thermal behavior of the collector are: $\eta_{0,b}$, K_b, K_d, a_1, a_2 and a_5. The first parameter is the optical efficiency of the collector at normal incidence referred to direct solar irradiance, a_1 and a_2 are the thermal loss factors, a_5 is the effective thermal capacity divided by the total area of the collector (A_G), and K_b and K_d are the incident angle modifiers (IAM – Incident Angle Modifier) for the direct and diffuse solar irradiance, respectively. All parameters are constant except for IAM for direct solar irradiance, K_b, which varies in relation to the angle of incidence of the direct beam, θ.

A novel parameterization for the QDT test of flat plate collectors was proposed and assessed in a previous study (Rodríguez-Muñoz et al., 2021b). This parameterization involves dividing the incident angle range into smaller intervals and assuming a piecewise linear function within each interval, taking the nodal values of the IAM as parameters to be determined. For instance, if a 10° interval is employed, the adjustable parameters would be $K_b(10°), K_b(20°), \ldots, K_b(80°)$, where $K_b(\theta_i)$ represents the K_b value at the angle θ_i (or node). Then the K_b value for any θ angle can be expressed as:

$$K_b(\theta) = \left[K_b\left(\left\lfloor\frac{\theta}{10}\right\rfloor 10\right)\left(\left\lfloor\frac{\theta+10}{10}\right\rfloor - \frac{\theta}{10}\right) + K_b\left(\left\lfloor\frac{\theta}{10}\right\rfloor 10 + 10\right)\left(\frac{\theta}{10} - \left\lfloor\frac{\theta}{10}\right\rfloor\right)\right], \tag{2}$$

where the open square brackets indicate to round up to the previous lower natural number. For all types of collectors it is mandated that $K_b(0°) = 1$ and $K_b(90°) = 0$ for the first and last parameters, respectively.

In Rodríguez-Muñoz et al. (2021b), it is shown how to integrate this equation into the QDT testing of flat plate collectors, and how to determine the nodal values using multilinear regression. This approach exhibited superior performance across a wide range of angles of incidence compared to other models (Souka & Safwat, 1966; Perers, 1997; Kalogirou, 2004; ISO-9806, 2017).

When dealing with evacuated tube collectors, the situation becomes more intricate, as K_b is a function of two angles of incidence, θ_L and θ_T, which correspond to the angles projected onto two perpendicular planes; one longitudinally along the tube axis and the other transversely across the tube, respectively. A significant simplification for this issue was introduced by McIntire (1982), involving the factorization of the IAM. This factorization expresses the IAM as the product of two distinct functions: one reliant on θ_L and the other on θ_T, denoted as $K_b = K_{bL} \times K_{bT}$. K_{bL} signifies K_b calculated at $(\theta_L, 0)$ and K_{bT} signifies K_b calculated at $(0, \theta_T)$. This assumption is widely accepted and commonly applied in tests involving this type of collector (Osório & Carvalho, 2014; Zambolin & Del Col, 2012). Typically, the parameterizations used to describe the IAM of flat plate collectors are applied to each IAM component of ETC technology.

In the present study, the same factorization assumption was adopted, and the recently proposed parameterization by Rodríguez-Muñoz et al. (2021b) for flat plate collectors was utilized for each IAM component of the ETC. To be more precise, the discretization process of Rodríguez-Muñoz et al. was applied to both the functions K_{bL} and K_{bT}. However, in this case, integrating this model into QDT testing is more complex, and the procedure used in this work is detailed in Subsection 2.5.

This article marks the first application of this parameterization for evacuated tube collectors with heat pipes, highlighting its generality across different technologies, particularly its applicability to collectors with biaxial IAM. As mentioned earlier, this model outperforms those currently available; therefore, the implementation of this model improves the accuracy of the IAM estimation for ETC.

2.2. SST model and parameters

The SST implementation provides the baseline reference for comparison with the enhanced QDT methods. For the SST methodology, the classical simpler model is used that deals globally with solar radiation, making the following substitution,

$$\eta_{0,hem} K_{hem} G_t = \eta_{0,b} \left[K_b \left(\theta \right) \; G_{bt} + K_d \; G_{dt} \right]. \tag{3}$$

This equation is considered valid under clear sky conditions, which are the conditions for conducting the SST test ($G_t > 700\,\mathrm{W/m^2}$ and a diffuse fraction less than 30 %, as specified by the standard). This substitution results in the following model,

$$\frac{\dot{Q}_u}{A_G} = \eta_{0,hem} K_{hem} G_t - a_1 \left(\vartheta_m - \vartheta_a \right) - a_2 \left(\vartheta_m - \vartheta_a \right)^2 - a_5 \frac{d\vartheta_m}{dt}, \tag{4}$$

where G_t is the global solar irradiance at the collector plane, and the parameters $\eta_{0,hem}$ and K_{hem} correspond respectively to the optical efficiency at normal incidence and the angle of incidence modifier, both related to the global solar irradiance. It is worth noting that in the SST model, the parameter C is commonly used to characterise the effective thermal capacity of the collector. However, in order to maintain homogeneity, a_5 was chosen instead. The relationship between C and a_5 is given by $a_5 = C/A_G$.

2.3. Conversion between SST and QDT

Annex B of ISO-9806 provides a procedure for estimating the parameters $\eta_{0,b}$, K_b and K_d from $\eta_{0,hem}$ and K_{hem}, and the reverse procedure, which is outlined below. The parameter K_d is calculated by averaging and normalising K_b over the solid angle seen by the collector, as shown in Eq. (5):

$$K_d = \frac{\int_0^{\pi/2} \int_0^{\pi/2} K_b \left(\theta, \gamma \right) \cos \left(\theta \right) \sin \left(\gamma \right) d\theta d\gamma}{\int_0^{\pi/2} \int_0^{\pi/2} \cos \left(\theta \right) \sin \left(\gamma \right) d\theta d\gamma}. \tag{5}$$

For this calculation, clear sky conditions are assumed as well as an isotropic distribution for diffuse solar irradiance. It is pointed out that the SST is done under clear sky conditions, as we mentioned before, conditions where the solar irradiance can be neglected and $K_{hem} = K_b$ can be reasonably assumed).

The ISO-9806 (2017) standard suggests performing this integral as a summation, discretising the integration domain by squares of 10° side, the approach used in this work. The parameter $\eta_{0,b}$ is then calculated from Eq. (3) assuming normal incidence and a diffuse fraction of 15 % in the plane of the collector, which is a reasonable assumption for SST conditions.

However, since there are differences in the IAM estimation between the SST and QDT methods, an improved parameter conversion method is proposed in this work, which, together with its advantages over the standard procedure, are presented in Subsection 4.4.

2.4. Test procedures

Table 1 shows the conditions required for each test method and for each variable, including the allowed variability. These conditions must be met by the measurements recorded during the test in order to be used for parameter identification. In particular, the SST methodology imposes more rigorous requirements, both in terms of the required values and their allowed variation. Conversely, the QDT methodology requires the representation of different weather conditions during the test. In the following subsection, a brief overview of both test methods is presented, with particular emphasis on the aspects relevant to the implementation of the QDT test method for evacuated tube solar collectors.

Table 1: Conditions and variability required for each test variable specified by the standard ISO-9806.

Variable	SST		QDT	
	Condition	Variability	Condition	Variability
Global solar irradiance G_t (W/m^2)	>700	±50	-	-
Diffuse fraction f_d (%)	<30	-	-	-
Incident angle θ (°)	<20	-	-	-
Inlet temperature ϑ_i (°C)	-	±0.1	-	±1
Outlet temperature ϑ_o (°C)	-	±0.4	-	-
Ambient temperature ϑ_a (°C)	-	±1.5	-	-
Wind velocity parallel to the collector u (m/s)	3±1	±1.0	<4	-
Mass flow rate $\dot{m}$ (kg/(s m^2))	0.02	±1 %	0.02	±2 %

2.4.1. Quasi dynamic testing method

For the QDT method, all parameters are determined by a single test, which involves performing at least one measurement sequence for each type of day, with each day type corresponding to a specific measurement sequence defined by the standard. The main objective of these day types is to operate the collector under various working conditions, such as different temperature differences and sky conditions. The total number of sequences required depends on the local climatic conditions and the time of year when the test is carried out. Each type of day must last at least 3 hours and may consist of several non-consecutive sub-sequences, each lasting at least 30 minutes. The conditions that the day types must meet in order to comply with the standard are described below:

- Day type 1: this sequence should be conducted with the fluid temperature kept as close as possible to the ambient temperature. The measurements should be carried out mostly under clear sky conditions. Additionally, the angle of incidence should vary within a defined range to ensure ample variability for the IAM for direct irradiance. This range should encompass incident angles exceeding 60° and extend to angles where the difference in the IAM for beam irradiance does not exceed 2 % from the value at normal incidence. This sequence contributes to the determination of the parameters related to the optical efficiency of the collector; $\eta_{0,b}$, K_b and K_d.

- Day type 2: during this measurement sequence, the collector should operate under conditions of varying cloudiness, and it can be conducted at any operating temperature. The high degree of variability in solar irradiance in these sequences contributes to the determination of the thermal capacity of the collector. To ensure an accurate determination of this parameter, the time derivative of the mean temperature of the fluid, $d\vartheta_m/dt$, must exceed the threshold value of $\pm 0.005\,°\mathrm{C/s}$. In addition, the measurement at low diffuse fraction also contributes to the determination of the IAM for the diffuse solar irradiance; K_d.

- Day type 3: in this sequence the collector must operate with an intermediate inlet temperature and the measurements must include clear sky conditions. At least two intermediate temperatures are needed (i.e., $(\vartheta_m - \vartheta_a)$ equal to 20 and 40 °C).

- Day type 4: in this sequence the collector must operate with a high inlet temperature and the measurements must include clear sky conditions (i.e., $(\vartheta_m - \vartheta_a)$ equal to 60 °C). The day type sequences 3 and 4 contribute to determining the thermal loss factors; a_1 and a_2.

To ensure that the experimental data set contains sufficient variability and different working conditions are achieved, the standard recommends the generation of the following diagnostic plots: 1) $(\vartheta_m - \vartheta_a)$ as a function of G; 2) G_{bt} as a function of θ; 3) G_{dt} as a function of G; and 4) $(\vartheta_m - \vartheta_a)$ as a function of u (the ambient air speed). These plots must be compared with the typical plots in the standard and should show a significant degree of similarity.

To improve the reliability of results, the following guidelines for ETC-HP testing are outlined, taking into account the specific characteristics of this technology. An effective approach for day type 1 would involve obtaining two measurement sequences: one with $\theta_L = 0°$ and θ_T varied from 0° up to angles exceeding 60°, and the converse for the second sequence (i.e., θ_L varied from 0° up to angles exceeding 60° and $\theta_T = 0°$). This decoupling of variables simplifies the determination of the functions K_{bL} and K_{bT}. In QAiST (2012), it is recommended to carry out these tests using an automatic solar tracker: in the first sequence, the tracker is fixed to the equator, and it follows the Sun's height, while in the second sequence, the tracker's horizontal inclination is fixed, and it tracks the Sun's azimuth. If an automatic solar tracker is not available (fixed or manually-operated support), the procedure described in Zambolin & Del Col (2012) can be followed. In this case, the collector support is fixed to the equator, and various measurement sequences are taken with different horizontal inclinations.

For this study, an intermediate procedure was adopted: in the initial sequence, the solar tracker's azimuth was aligned North (as it is located in the Southern Hemisphere), while the horizontal inclination was set at 45° ($\theta_L < 20°$, $\theta_T = 0$–$70°$). In the second sequence, the tracker was adjusted to track the Sun's azimuthal position ($\theta_L = 0$–$50°$, $\theta_T = 0°$), and the horizontal inclination was fixed at 30°. These selections of horizontal inclinations were not arbitrary but meticulously chosen for the specific location and moment of the year to ensure that $\theta_L < 20°$ was attained in the first sequence and $\theta_L = 0$–$50°$ in the second sequence, encompassing the most substantial achievable variation during the test's time of execution.

Regarding day type 2, the requirement of ±0.005 °C/s poses a challenge for ETC collectors due to the specific characteristics of the technology, such as slow thermal response and low temperature difference between the inlet and outlet. To address this issue, we recommend that this test is performed at a low temperature to maximise temperature variation (although even with this approach it may still be difficult to meet the requirement).

For day type 4, while a temperature difference of $(\vartheta_m - \vartheta_a) = 60$ °C may be suitable for many collectors, it may not be sufficient for tube collectors due to their low thermal loss coefficient. This can make the identification of the parameter a_2 difficult. In this respect, it is recommended to run this type of day with the highest possible temperature difference. Subsequently, the intermediate temperatures corresponding to day type 3 should be chosen so that the separation between all test temperatures is as uniform as possible.

In addition, two important points are highlighted regarding the installation of these collectors before the tests are carried out. Firstly, the back of the collector should be shielded from any solar radiation that may be reflected from the ground and/or adjacent surfaces. This type of collector is susceptible to this back solar radiation, which can affect the results, even if the surfaces have a low reflectivity. Secondly, it is important that the tubes of the collector are well aligned, that is, the structure of the collector should be squared and aligned with the test bench, otherwise erroneous results may be obtained in the IAM (small misalignment in flat collectors are not a problem as their IAM is uniaxial).

2.4.2. Steady state testing method

In the case of the SST method, parameter identification involves three independent tests: (i) the performance test, where the parameters $\eta_{0,hem}$, a_1 and a_2 are determined; (ii) the incident angle modifier test, where K_{hem} is determined; and (iii) the effective thermal capacity test, where the parameter a_5 is determined. The first test is well documented and extensively discussed in several references (Rojas et al., 2008) and therefore a detailed description is not necessary.

For the second test (IAM determination), the same procedure as for day 1 of the QDT test was followed, but the experimental data were processed according to the standard for this method. For each angle of incidence, the experimental IAM value was determined using Eq. (4), assuming steady state conditions ($d\vartheta_m/dt \approx 0$),

$$K_{hem}(\theta) = \frac{\dot{Q}_u/A_G + a_1\,(\vartheta_m - \vartheta_a) + a_2\,(\vartheta_m - \vartheta_a)^2}{\eta_{0,hem}\,G_t}. \tag{6}$$

The final value of the IAM for a given angle of incidence was calculated as the average of two measurements: one before and one after solar noon (symmetrical), to account for transient effects.

The effective thermal capacity test was carried out in accordance with section 25.2 of the ISO-9806 (2017) standard, taking into account the second-order correction for thermal losses, i.e. the a_2 coefficient. At the beginning of the test, the inlet temperature was set equal to the ambient temperature and the collector was covered with a reflective blanket to reach steady state. The cover was then removed and the collector was allowed to reach a new steady state point, which differed from the initial one due to the effect of solar irradiance. The effective thermal capacity was determined by integrating Eq. (4) over the period between the two steady state operating points, assuming normal incidence ($K_{hem} \approx 1$),

$$a_5 = \frac{\int_{t_1}^{t_2} \left[\eta_{0,hem} G_t - a_1 \left(\vartheta_m - \vartheta_a \right) - a_2 \left(\vartheta_m - \vartheta_a \right)^2 - \dot{Q}_u / A_G \right] \, dt}{\vartheta_{m2} - \vartheta_{m1}}. \tag{7}$$

All these SST stages were done as standard as possible, following closely the ISO-9806 (2017), so they act as a baseline reference to compare with the QDT method's results under the proposed framework.

2.5. Parameter identification algorithm for QDT

There are two parameter identification procedures (Fischer et al., 2004): (i) the finite difference time derivative approximation and (ii) the dynamic parameter identification. In both cases, the mean square error of the useful power is used as the objective function to be minimised. The first method is the most commonly used and the one used in this study. It involves the approximation of the time derivative of the mean temperature of the fluid using finite differences, as follows:

$$\frac{d\vartheta_m}{dt} \cong \frac{\vartheta_m(t + \Delta t) - \vartheta_m(t)}{\Delta t}. \tag{8}$$

where Δt is the data averaging time, $\vartheta_m(t)$ and $\vartheta_m(t + \Delta t)$ correspond to the average temperature of the fluid at the beginning and end of the time interval Δt. The term $d\vartheta_m/dt$ is then an additional independent variable within the regression algorithm. The time interval Δt corresponds to the averaging time of the experimental data.

The implementation of the MLR (Multi Linear Regression) method is widely used in the literature for flat plate collectors because the regression problem can be expressed in linear form (Perers, 1997). However, when dealing with ETC collectors, the problem becomes nonlinear due to the characteristics of the IAM. Some studies have proposed to deal with this nonlinearity by using the MLR method in an iterative way (Hofer et al., 2015). In this study, we opt for the direct implementation and propose the use of a constrained nonlinear regression algorithm. Although this method is more challenging to implement, it is a more appropriate approach to deal with the nonlinearity of the problem. In addition, once implemented, it does not require iteration or manual parameter substitution, which simplifies its use and reduces the risk of error.

The nonlinear regression algorithm used in this work is known as the two-metric projection method (Bertsekas, 1999). The projection is used to incorporate the constraints and ensure that the parameters converge to physically possible values. The algorithm consists of six steps, which are summarized as follows.

Since this algorithm is iterative, it starts with an assumed vector of characteristic parameters, denoted p_0. This vector includes all the characteristic parameters of Eq. (1) and the IAM: $\eta_{0,b}$, K_d, a_1, a_2, a_5, $K_{bL}(10°, 0)$, $K_{bL}(20°, 0)$, …, $K_{bL}(80°, 0)$, $K_{bT}(0, 10°)$, $K_{bT}(0, 20°)$, …, $K_{bT}(0, 80°)$.

The second step involves evaluating the function $\dot{Q}_u^*(p)$ at p_0, specifically calculating $\dot{Q}_u^*(p_0)$. This function represents the estimated useful power produced by the collector, calculated using Eqs. (1) and (8) and the measured variables. In this step, the associated error of this estimation is also computed, denoted $E(p_0)$ and calculated as $E(p_0) = \dot{Q}_u^*(p_0) - \dot{Q}_u$, where $\dot{Q}_u$ represents the experimentally measured useful power produced by the collector.

The useful power produced by the collector is then linearized around this initial operating point, as shown in Eq. (9).

$$\dot{Q}_u^*(p) \approx \dot{Q}_u^*(p_0) + J(p_0)\,(p - p_0)\,. \tag{9}$$

The Jacobian $J(p_0)$ represents the derivatives of the function $\dot{Q}_u^*(p)$ with respect to the characteristic parameters, evaluated at the point p_0. The entries of $J(p_0)$ can be estimated numerically using centred finite differences,

$$J(p_0)_{i,j} = \frac{\partial \dot{Q}_u^*(t_i, p_0)}{\partial p_j} = \frac{\dot{Q}_u^*(t_i, p_0 + \delta p_j) - \dot{Q}_u^*(t_i, p_0 - \delta p_j)}{2\delta p_j}. \tag{10}$$

For δp_j, the value suggested by Bates & Watts (1988) was used, that is, $\delta p_j = \sqrt{\epsilon} p_j$, where ϵ is the epsilon machine. The computation of the matrix $J(p_0)$ represents the third step of the algorithm.

The fourth step of the algorithm involves identifying the active constraints. To do this, the auxiliary vector $\tilde{p}$ is computed using gradient descent algorithm,

$$\tilde{p} = p_0 - \alpha\, J(p_0)^\top\, E(p_0), \tag{11}$$

where α is the step size of the gradient descent algorithm, which is set to a very small number ($\alpha = 10^{-10}$). To identify the active constraints, simply examine the entries of the vector $\tilde{p}$ and check if they exceed the established limits. If so, the constraint associated with that entry is considered active.

The fifth step involves estimating the Hessian matrix of the function $\dot{Q}_u^*(p)$ around p_0, denoted $S(p_0)$. This matrix is initially estimated using the linearization hypothesis as shown below,

$$S(p_0) = \left[J(p_0)^\top J(p_0)\right]^{-1}. \tag{12}$$

Then, when a constraint is active, the corresponding row and column in this matrix are set to zero, except for the element on the diagonal, which is set to one.

In the sixth and final step, the parameter's vector in the next iteration step is calculated as follows,

$$\hat{p} = \texttt{Proy}\left\{p_0 - S(p_0)\,J(p_0)^\top\,E(p_0)\right\}, \tag{13}$$

where $\texttt{Proy}\{\}$ is the projection function over the range of physically possible parameter values. Experimental errors can cause some parameters to take on values that are inconsistent with their physical meaning. To address this problem, certain constraints have been imposed: $a_2 \geq 0$ and $K_{bL} \leq 1$, which are box-type constraints. For a deeper understanding of these parameters and the rationale behind these constraints, the reader can refer to Duffie & Beckman (1991) and Theunissen & Beckman (1985). The latter gives an estimate of the IAM for tubular collectors using ray tracing and shows, among other things, that $K_{bL} \leq 1$. The implementation of the projection function in this case is straightforward. If one of the parameters exceeds the defined limits, it is assigned the closest limit value (e.g. if $a_2 < 0$, then a_2 is set to 0). The iteration process continues until the difference in the parameter vector $\hat{p}$ between one iteration and the next becomes negligible (less than a certain tolerance, set to 0.1 % is this work).

A drawback of this algorithm is that it may converge to a local minimum instead of the global minimum. To address this issue, the procedure is iterated with 10 different randomly generated initial points (p_0). In cases where the algorithm converges to different solutions, the solution with the smallest mean square error (representing the global minimum) is selected. The linearisation approach is used to estimate parameter uncertainties, as shown in Hofer et al. (2015); Rodríguez-Muñoz et al. (2021b).

3. Test facilities and experimental data

In this section, the test setup and the measurements taken for parameter identification are described.

3.1. Test facilities and collectors

The tests were carried out at the Solar Heater Test Bench (Banco de Ensayos de Calentadores Solares - BECS) of the Solar Energy Laboratory (Laboratorio de Energía Solar - LES, http://les.edu.uy/) of the University of the Republic (Udelar), located in Salto, Uruguay (latitude=31.28° S, longitude=57.92° W). This test facility was designed by researchers from this laboratory, based on existing facilities from the National Renewable Energy Centre (Centro Nacional de Energías Renovables - CENER) in Spain. This installation, including the thermo-hydraulic system, measurement instruments, and data acquisition systems, is described in detail in Rodríguez-Muñoz et al. (2021b).

It should be noted that recently, this testing capacity participated in a Latin American Laboratory Intercomparison organised by PTB (Physikalisch-Technische Bundesanstalt), the German Metrology Institute, and supported by Solar und Wärmetechnik Stuttgart (SWS, Germany), where it obtained the highest rating in most of the test variables and received only two minor observations regarding secondary variables, which were already addressed by the laboratory (Fischer, 2020).

For this study, two evacuated tube solar thermal collectors with heat pipes were considered, designated ETC-HP-1 and ETC-HP-2, with gross areas A_G of 1.79 m^2 and 1.55 m^2, respectively. The gross area corresponds to the maximum projected area of the complete collector, excluding any integral means of mounting and connecting fluid piping, as specified in ISO-9488 (2022). Both collectors were mounted on a mobile tracker with a manually adjustable horizontal tilt and an azimuth that could be adjusted either manually or automatically at 2-minute intervals. Figure 1 shows the assembly of the ETC-HP-1 collector in the test facility as an example. In this figure, the black cover behind the collector, which is used to prevent solar radiation reflection from the ground, can be seen. The tracker was configured during the tests according to the procedures described in Subsection 2.4. ETC-HP-1 was tested from 18 August to 4 October 2021, while ETC-HP-2 was tested from 3 September to 30 September 2022.

Figure 1: Assembly of the collector ETC-HP-1 on the solar tracker of the test bench.

The design of the collectors is standardized, so they share several similarities. They both utilize borosilicate tubes with an outer diameter of 59 mm and a length of 1.80 m. Additionally, both collectors are equipped with heat pipes featuring metal cylindrical fin absorber. For a better understanding of the different evacuated collector technologies, particularly the one used in this work, please refer to Kumar et al. (2021). The heat pipes measure 168.7 cm in length, with 163 cm designated for the condenser section and 5.7 cm for the evaporator section. The diameters of the condenser and evaporator in both collectors are 14 mm and 8 mm, respectively.

The main difference between ETC-HP-1 and ETC-HP-2 lies in the number of tubes and their spacing. The ETC-HP-1 consists of 8 tubes, spaced 52 mm apart, while the ETC-HP-2 has 10 tubes with a smaller spacing of 18 mm between them. The larger spacing of ETC-HP-1 is due to its design for use with compound parabolic concentrators (CPCs), although in this case, it is used without them. The difference in spacing gives rise to different IAMs, which makes them of interest for the evaluation of the proposals presented in this article (novel IAM for QDT method and improved parameter conversion for SST method).

3.2. Data set description

The tests were carried out according to the ISO-9806 (2017) standard. During the tests, a wind speed of 3 m/s (spatial average) was maintained using fans. In addition, the mass flow rate was set to 2.00 kg/min for ETC-HP-1 and 1.90 kg/min for ETC-HP-2 due to the different collector gross area, in accordance with ISO-9806 (2017), 0.02 kg/(s m^2) approximately. From the tests carried out, 6 different measurement sequences were obtained for each collector using the QDT method. Table 2 summarises the main characteristics of the measurement sequences for each collector. The table shows the date of each test, the inlet temperature ϑ_i (average, and maximum variability between brackets), the flow rate $\dot{m}$ (average and maximum variability, the latter in percent), the average temperature difference $\vartheta_m - \vartheta_a$, the diffuse fraction $f_d = G_{dh}/G_h$ (range of variation) and the transverse and longitudinal angles of incidence (range of variation). All sequences meet the temperature and flow rate stability requirements at the collector inlet as specified in the ISO-9806 (2017) standard for the QDT method (variability less than ±1 °C and 2 % of the mean, respectively). Appendix A shows the required figure checks according to the standard for the ETC-HP-1 collector as an example. The plots for ETC-HP-2 were omitted because they are very similar to those for ETC-HP-1 and do not provide any additional information.

Table 2: Description of the measurement sequences conducted for the QDT method on each collector.

Collector	Sec.	Date	Hour	Dur.	ϑ_i (°C)	$\dot{m}$ (kg/min)	$\vartheta_m - \vartheta_a$ (°C)	f_d	θ_L (°)	θ_T (°)
ETC-HP-1	1a	30/08/2021	08:05-17:55	09:50	27.1(0.49)	1.984(1.19)	4.3	0.09-0.32	0-13	0-72
	1b	04/10/2021	07:35-17:40	10:05	20.2(0.48)	1.987(0.34)	3.4	0.07-0.14	0-46	0
	2a	28/08/2021	11:25-14:25	03:00	22.2(0.15)	1.985(1.14)	2.2	0.25-0.95	0-5	0-24
	3a	18/08/2021	11:25-14:25	03:00	53.3(0.19)	1.964(1.02)	27.3	0.22-0.26	0-4	0
	3b	11/09/2021	11:25-14:25	03:00	64.6(0.18)	1.953(1.08)	46.2	0.07-0.37	0-10	0-25
	4a	27/08/2021	11:25-14:25	03:00	89.6(0.14)	1.922(1.03)	72.0	0.10-0.12	0-4	0
ETC-HP-2	1a	07/09/2022	07:50-17:15	09:25	22.9(0.49)	1.885(0.56)	3.0	0.12-0.26	0-8	0-72
	1b	27/09/2022	08:05-17:15	09:10	24.9(0.20)	1.887(0.62)	2.6	0.10-0.13	0-40	0
	2a	30/09/2022	11:30-14:30	03:00	23.0(0.16)	1.887(0.52)	2.5	0.17-0.99	0-18	0
	3a	04/09/2022	12:50-15:50	03:00	45.9(0.11)	1.873(0.28)	29.0	0.10-0.10	0-12	0
	3b	05/09/2022	12:50-15:50	03:00	66.9(0.17)	1.853(0.46)	47.0	0.09-0.10	0-12	0
	4a	03/09/2022	12:50-15:50	03:00	88.5(0.15)	1.828(0.77)	72.4	0.09-0.09	0-12	0

The SST method used the same data set, but it is subject to the specific processing procedures for this method, identifying the sub-sequences or data points that meet the measurement requirements shown in Table 1. Sequences 1a, 3a, 3b and 4a were used for the performance test, representing data under clear sky conditions and around solar noon (low angle of incidence). Sequences 1a and 1b were used to determine the IAM, and an additional test of the effective thermal capacity was performed by covering and uncovering the collector as described in section Subsection 2.4.2.

It is noted that the number of data points per day type and their distribution may vary from one implementation to another, and the tests may still be valid. Table 2 and the figures in Appendix A illustrate our specific implementation of the QDT method, and they are provided as examples to facilitate the reproduction of the method by other laboratories.

4. Results

This section presents and discusses the main scientific results of this work. Subsection 4.1 validates the novel IAM model for the QDT method by comparison with the SST method, and provides a detailed analysis of the discrepancies between the test methods. In this context, Subsection 4.2 shows the effect of these discrepancies on the useful power produced by the collector. Subsection 4.3 illustrates the dependence of QDT results on the averaging time of the experimental data and reveals the optimal value that improves the reliability of the results for the QDT methodology. Finally, Subsection 4.4 proposes and evaluates an alternative method to convert SST parameters to QDT.

4.1. Validation of the novel IAM model and comparison between test methods

Table 3 shows the coefficients of the thermal models from Eq. (1) for each test method and their respective typical uncertainty. The same IAM model is used for both test methodologies. Also, the proposed non-linear fit strategy based on the two-metric projection is used for the QDT. It should be noted that the parameters are referred to the gross area of the collectors, as required by the test standard. For this reason, the optical efficiency is relatively low compared if the absorption area is used as a reference. The values of the nodes for the angle of incidence modifier are reported every 10 degrees, where K_{bL} for $\theta_L > 40°$ and K_{bT} for $\theta_T = 80°$ are interpolated values, as commonly done for these angle values. For the QDT method, the characteristic parameters were determined for three different averaging times: 1, 5, and 10 minutes. The 10 minute averages were used for Table 3, as they minimize the difference with the results from the SST methodology (which will be further discussed in Subsection 4.3).

For all parameters, a t-statistic exceeding 3 was acquired, indicating statistical significance, except for the parameter a_2, which therefore had to be held constant at 0. In most instances, the disparities between values obtained from either method were below 10%, except for parameters K_{bT} for $\theta_T > 50°$, K_d, and a_5, which are elaborated upon in subsequent sections. It is important to highlight that despite these variations,

Table 3: Characteristic parameters of the tested collectors obtained through SST and QDT methodologies. Data not applicable is indicated by N/A.

Collector	ETC-HP-1				ETC-HP-2			
Method	SST		QDT		SST		QDT	
	Value	Uncer.	Value	Uncer.	Value	Uncer.	Value	Uncer.
$\eta_{0,hem}$	0.274	±0.002	N/A	N/A	0.371	±0.003	N/A	N/A
$\eta_{0,b}$	0.274	N/A	0.262	±0.001	0.371	N/A	0.367	±0.003
K_d	1.013	N/A	1.257	±0.023	1.007	N/A	1.181	±0.033
a_1	1.211	±0.041	1.255	±0.029	1.682	±0.060	1.686	±0.044
a_2	0	0	0	0	0	0	0	0
$a_5 \times 1000$	122.3	±1.1	65.0	±4.0	207.6	±1.0	126.0	±4.0
$\theta_L \backslash \theta_T$	K_{bL}	K_{bT}	K_{bL}	K_{bT}	K_{bL}	K_{bT}	K_{bL}	K_{bT}
0	1,00	1,00	1.00	1.00	1,00	1,00	1.00	1.00
10	0,98	0,98	1.00	1.02	0,99	1,01	0.98	1.01
20	0,98	1,03	1.00	1.10	0,99	1,07	1.00	1.07
30	0,98	1,12	1.00	1.15	1,00	1,15	1.00	1.20
40	0,94	1,25	1.00	1.33	0,97	1,29	0.93	1.39
50	0,75	1,46	0.78	1.56	0,77	1,40	0.74	1.58
60	0,57	1,76	0.59	2.08	0,58	1,44	0.56	1.57
70	0,38	1,62	0.39	2.35	0,39	1,18	0.37	1.68
80	0,19	0,81	0.20	1.18	0,19	0,59	0.19	0.84
90	0	0	0	0	0	0	0	0

the obtained values are consistent with those reported in other literature for collectors of the same technology (Osório & Carvalho, 2014; Zambolin & Del Col, 2012). This validates the implementation of the novel IAM model.

It is noted that in (Rodríguez-Muñoz et al., 2021b) the performance of this model has already been compared with that of other models (Souka & Safwat, 1966; Perers, 1997; Kalogirou, 2004; ISO-9806, 2017), and its superiority has been demonstrated for flat plate collectors. In the aforementioned work, two independent data sets of a flat plate collector are used: one to adjust the parameters of the models and another to evaluate their performance using metrics such as root mean square error and mean bias. In this sense, the novel model shows better performance over the entire range of incidence angles, indicating superior accuracy. IAM models typically extend from those used for flat plate collectors to tube collectors; therefore, we are confident that the superiority of the proposed model remains in the context of ETC collectors.

Next, the differences obtained in the parameters K_{bT} for $\theta_T > 50°$, K_d, and a_5 are discussed in greater detail, aiming to guide future research in the area and thereby improve testing standards in general, especially for this type of technology. Some of these differences are partially addressed in the following sections.

In the case of $K_{bT}(\theta_T > 50°)$, the differences between the SST and QDT methods increase with the angle of incidence and range from 9 % to 45 %. These differences can be attributed to two main factors. First, as the angle of incidence increases, the useful power produced by the collector decreases, leading to higher relative uncertainty and variability in the IAM determination. Second, the SST method does not distinguish between direct and diffuse solar irradiance, but works with global solar irradiance, and the determined IAM (K_{hem}) refers to the latter. Since the SST test is performed under clear sky conditions (low diffuse fraction, less than 30 %), the standard assumes $K_{hem} = K_b$. This suggests that the IAM obtained by the QDT should be a more reliable estimate, as it incorporates the separate modeling of direct and diffuse solar irradiance.

Regarding the parameter K_d, the difference is about 18 % for both collectors, and in both cases the value of K_d estimated by the SST method is lower than the one determined experimentally by the QDT method. This discrepancy has also been reported in other publications for both flat plate collectors and evacuated tube collectors Kovács et al. (2011); Osório & Carvalho (2014); Rodríguez-Muñoz et al. (2021b) (note that Osório & Carvalho (2014) does not report the value of K_d for the SST method, but it can be estimated by integrating the values of K_{hem} using Eq. (5)). We attribute the discrepancy in K_d to two reasons derived from the assumptions underlying Eq. (5): 1) $K_{hem} = K_b$, and 2) the isotropic behavior of the diffuse solar irradiance. The first assumption was discussed in the previous section. The second assumption is valid under cloudy sky conditions, but not under partly cloudy and clear sky conditions, as shown in Brunger & Hooper (1993); Rodríguez-Muñoz et al. (2021c). The IAM test for the SST method is performed under clear sky conditions and requires measurements throughout the day if performed with a fixed tracker (with varying solar altitude throughout the day), so neither of these assumptions is fully satisfied during the test. On the other hand, the value of K_d in the QDT method is determined directly from the experimental data, taking into account the anisotropic effects of diffuse solar irradiance and the varying sun positions during the test. This creates a clear contrast in the treatment of K_d between the two test methods. In an effort to improve the compatibility between the two methods, in Subsection 4.4 we propose an alternative method for converting SST and QDT parameters, taking into account the diffuse fraction during the IAM test of the SST method, which provides parameters more similar to those of the QDT method.

Finally, for the parameter a_5 (effective thermal capacity per unit of gross area), differences of 40 % and 89 % were found, with the value obtained by the SST method being higher. This behavior was also observed previously by Osório & Carvalho (2014). Moreover, the obtained values seem high if we consider the physical composition of the collectors. If we weigh the mass and specific heat of the materials that make up the collectors (according to section 25.4 of ISO-9806 (2017)), we obtain a_5 values of $4080\,\mathrm{J/°Cm^2}$ and $5459\,\mathrm{J/°Cm^2}$ for collectors ETC-HP-1 and ETC-HP-2, respectively. The significant difference from these values raises doubts about the reliability of the test methods for determining the thermal capacity of this type of collectors. This is not the case for flat plate collectors, where similar thermal capacity values are obtained using different test methods or estimates (Osório & Carvalho, 2014; Rodríguez-Muñoz et al., 2021b). In addition, it is worth mentioning that in most calculations of the energy produced by the collectors, steady-state conditions are assumed, which makes the value of the thermal capacity less important. However, in the QDT method, the determination of the parameters is global, i.e. all parameters are determined at the same time, so an error in the determination of a_5 could lead to errors in the determination of the other parameters. For this reason, improving the test methods for determining a_5 is relevant future work.

4.2. Useful power under standard reporting conditions

In addition to the results presented in the previous section, the useful power produced by the collector was calculated for each case using Eq. (1), assuming normal incidence and steady-state conditions, for different temperature and sky conditions. The Standard Reporting Conditions (SRC) specified in the ISO-9806 (2017) standard were used for the different sky conditions. The results are shown in Table 4 together with the temperature and cloudiness conditions defined by the standard.

Table 4: Useful power produced by the collectors tested under standard reporting conditions. Calculations are done assuming normal incidence and steady-state conditions.

Collector	$\vartheta_m - \vartheta_a$ (°C)	Blue Sky $G_{bt} = 850\,\mathrm{W/m^2}$ $G_{dt} = 150\,\mathrm{W/m^2}$			Hazy Sky $G_{bt} = 440\,\mathrm{W/m^2}$ $G_{dt} = 260\,\mathrm{W/m^2}$			Gray Sky $G_{bt} = 0\,\mathrm{W/m^2}$ $G_{dt} = 400\,\mathrm{W/m^2}$		
		SST	QDT	Diff	SST	QDT	Diff	SST	QDT	Diff
ETC-HP-1	0	274	272	1 %	192	201	−4 %	111	132	−17 %
	20	260	247	1 %	168	176	−4 %	87	107	−21 %
	40	250	222	2 %	144	151	−5 %	62	82	−27 %
	60	226	197	2 %	120	126	−5 %	38	56	−39 %
ETC-HP-2	0	371	377	−1 %	260	274	−5 %	149	173	−15 %
	20	338	343	−2 %	227	240	−6 %	116	140	−19 %
	40	304	310	−2 %	193	207	−7 %	82	106	−25 %
	60	270	276	−2 %	159	173	−8 %	49	72	−39 %

For blue sky conditions, the difference in useful power is not very significant; between 1 and 2 % for collector ETC-HP-1 and less than 2 % for collector ETC-HP-2. However, the differences become more noticeable as cloudiness increases, reaching values between 4 % and 8 % for hazy sky and between 15 % and 39 % for grey sky conditions. Moreover, in all cases, the differences increase with the temperature difference. This difference is mainly attributed to the variation in the incidence angle modifier for diffuse irradiance, K_d. The impact of these differences on annual simulations will depend on the climate considered and the proportion of clear, partly cloudy, and overcast days. For instance, if the proportions of these days were equally distributed, differences ranging from 4 % and 11 % would be expected (average of the differences in Table 4, weighted by solar irradiance). It is anticipated that in arid and temperate climates, the difference will be much smaller due to the prevalence of clear and partly cloudy days over overcast days. This analysis shows the expected discrepancies in the useful power estimation due to different parameters' determination with the SST and QDT methodologies.

This study makes it clear that the differences obtained in the estimation of the parameter K_d with each testing method have a significant impact on the prediction of the useful energy of the collectors. Therefore, improving the estimation of this parameter constitutes an aspect to be enhanced in the standard. In this regard, in Subsection 4.4, an improved method is proposed to estimate the parameter K_d using the SST method, which partially reduces the differences with the QDT method.

4.3. Impact of the averaging time of experimental data on QDT method

In a previous study (Rodríguez-Muñoz, 2021), the effect of averaging time in the quasi-dynamic test of flat plate collectors was investigated. The results showed that most of the parameters remained almost constant regardless of the averaging time, with the exception of the parameter a_5. The value of this parameter showed an increasing trend with averaging time, reaching a stable value close to that obtained by the SST method after approximately 5 minutes of averaging. In addition, it was observed that the uncertainty of the parameters also increased with longer averaging times. Based on these results, it was concluded that an averaging time of 5 minutes was the most appropriate for this particular technology. However, this issue has not yet been analyzed for evacuated tube solar collectors with heat pipes.

Table 5 presents the parameter values for the collectors obtained with three different averaging times: 1, 5 and 10 minutes. Regarding the criteria for selecting these specific averaging times, earlier versions of the standard recommended a 5-10 minute interval; however, the current version has removed this guideline, leaving the choice open. We initially considered the 5 and 10 minute intervals based on past recommendations. Averaging times longer than 10 minutes were deemed impractical due to excessive data smoothing, which can distort the dynamics of the time series. In contrast, shorter times below 5 minutes capture more pronounced dynamic effects. However, times under 1 minute, such as 30 seconds, may introduce experimental errors due to the 10 second data acquisition frequency used in this work, as shown by Rodríguez-Muñoz (2021). Therefore, we selected 1, 5, and 10 minute intervals for simplicity. The results indicate that further exploration of additional time intervals is unnecessary.

The behavior of the parameters can be divided into three different groups. The first group includes parameters such as $\eta_{0,b}$, K_d, a_1, $K_{bT}(\theta_T \leq 50°)$, and $K_{bL}(\theta_L \leq 50°)$. As the averaging time increases, the values of these parameters tend to approach the corresponding values obtained by the SST method. The second group includes the parameters $K_{bT}(\theta_T > 50°)$ and $K_{bL}(\theta_L > 50°)$. In this case, the values deviate further from the corresponding SST values as the averaging time increases. The third and final group

Table 5: Characteristic parameters according to the QDT method for different averaging times.

Collector	ETC-HP-1						ETC-HP-2					
Method	1 minute		5 minute		10 minute		1 minute		5 minute		10 minute	
	Value	Uncer.	Value	Uncer.	Value	Uncer.	Value	Uncer.	Value	Uncer.	Value	Uncer.
$\eta_{0,b}$	0.258	±0.001	0.260	±0.0012	0.262	±0.001	0.350	±0.003	0.365	±0.003	0.367	±0.003
K_d	1.350	±0.013	1.306	±0.022	1.257	±0.023	1.479	±0.032	1.215	±0.038	1.181	±0.033
a_1	1.246	±0.016	1.244	±0.027	1.255	±0.029	1.452	±0.040	1.616	±0.051	1.686	±0.044
a_2	0.00	0	0.00	0	0.00	0	0.00	0.00	0.00	0.00	0.00	0.00
$a_5 \times 1000$	4	±0.4	46	±2.0	65	±4.0	14	±0.9	108	±3.0	126	±4.0
$\theta_L \backslash \theta_T$	K_{bL}	K_{bT}	K_{bL}	K_{bT}	K_{bL}	K_{bT}	K_{bL}	K_{bT}	K_{bL}	K_{bT}	K_{bL}	K_{bT}
0	1.00	1.00	1.00	1.00	1.00	1.00	1.00	1.00	1.00	1.00	1.00	1.00
10	1.00	0.98	1.00	1.01	1.00	1.02	0.93	1.05	0.97	1.02	0.98	1.01
20	1.00	1.08	1.00	1.09	1.00	1.10	0.80	1.13	0.98	1.11	1.00	1.07
30	1.00	1.16	1.00	1.14	1.00	1.15	1.00	1.21	1.00	1.20	1.00	1.20
40	1.00	1.33	1.00	1.34	1.00	1.33	0.99	1.40	1.00	1.39	0.93	1.39
50	0.95	1.60	0.80	1.56	0.78	1.56	0.80	1.55	0.80	1.56	0.74	1.58
60	0.71	2.07	0.60	2.10	0.59	2.08	0.60	1.59	0.60	1.60	0.56	1.57
70	0.47	2.12	0.40	2.22	0.39	2.35	0.40	1.48	0.40	1.51	0.37	1.68
80	0.24	1.06	0.20	1.11	0.2	1.18	0.2	0.74	0.2	0.76	0.19	0.84
90	0	0	0	0	0	0	0	0	0	0	0	0

consists only of the parameter a_5, which shows a continuous increase with the averaging time and does not seem to stabilize within the analyzed time interval. However, it remains consistently below the SST value (although, as explained before, this value may not be an appropriate reference for this type of collector). Similar to the findings for flat plate collectors, the uncertainty of the parameters also increases with longer averaging times for evacuated tube collectors.

Taking the SST results as a baseline considering that the parameters in the first group have a more substantial impact on the calculation of useful energy (under steady-state conditions, as is typically assumed), it can be concluded that an averaging time of 10 minutes is the most suitable in this case.

However, it is important to acknowledge that the significant variability of results with averaging time is a drawback of the QDT method. Therefore, improving this aspect is an area for future work. A possible alternative could be the adoption of dynamic identification algorithms, which have been successfully implemented in transient testing of other technologies and have shown advantages in modeling the transient effects of collectors (Spirkl et al., 1997; Hofer et al., 2015; Fahr et al., 2018; Rodríguez-Muñoz et al., 2021a). The use of dynamic algorithms is an interesting alternative to overcome some of the limitations associated with the current quasi-dynamic testing approach and to achieve more consistent and reliable results over different averaging times.

4.4. Enhanced parameter conversion procedure SST to QDT

As mentioned earlier, the parameter conversion between SST and QDT methods assumes the hypothesis that $K_{hem} = K_b$. However, this assumption may lead to differences in the estimation of the IAM between the SST and QDT methods, especially at low solar positions when the angle of incidence on the collector's plane is high, such as during sunrise and sunset. In this section, an alternative method is proposed to perform this conversion, taking into consideration the diffuse fraction during the test, and providing values more similar to those obtained through the QDT methodology.

Let's begin by considering Eq. (3), from which we can express the incidence angle modifier for direct irradiance, K_b, as follows,

$$K_b = \frac{\frac{\eta_{0,hem}}{\eta_{0,b}} K_{hem} - K_d\ f_d}{1 - f_d}. \tag{14}$$

Using this equation, it would be possible to calculate K_b from the measurements of K_{hem} under steady-state conditions. However, to do this, we need to know the diffuse fraction during the test and the values of the parameters $\eta_{0,hem}$, $\eta_{0,b}$, and K_d. While the diffuse irradiance is measured during the SST test, obtaining the values of $\eta_{0,b}$ and K_d poses a challenge as they are determined from K_b.

The alternative method proposed in this work involves an iterative process to determine K_b, $\eta_{0,b}$, and K_d. The procedure is described as follows. Firstly, we assume initial values for $\eta_{0,b}$ and K_d (initial seed). Next, we calculate K_b using Eq. (14), and subsequently, we recalculate the parameters $\eta_{0,b}$ and K_d. The initial seed values can be taken from the assumption that $K_{hem} = K_b$. The iterative process continues until the difference between the input and output parameters is less than a certain tolerance. This iterative approach helps refine the parameter values and provides a method to convert parameters between the SST and QDT methodologies, accounting for the influence of the diffuse fraction during the test.

Table 6 shows the results of the proposed procedure for the collectors ETC-HP-1 and ETC-HP-2 and compares them with the standard conversion method and the QDT results. The following trend can be observed: the proposed method produces lower IAM values when $K_b < K_d$ and higher values when $K_b > K_d$. The differences increase with higher separation between K_b and K_d and higher diffuse fraction. When compared with the results of the QDT method, it is observed that the proposed method gives more similar results, going from differences between 9 % and 45 % to differences between 8 % and 26 %. The increase in similarity occurs at high angles of incidence. The same happens with the parameters $\eta_{0,b}$ and K_d, for which the difference between the test methods is reduced. It is also observed that with the new set of parameters $\eta_{0,b}$ and K_d the difference in the useful power values under standard reporting conditions is reduced, between 1 % and 7 % percentage points depending on the temperature difference.

Table 6: Comparison of the standard procedure for conversion of SST to QDT parameters with the proposed procedure.

Collector	ETC-HP-1						ETC-HP-2					
Method	standard conversion		proposed conversion		QDT		standard conversion		proposed conversion		QDT	
$\eta_{0,b}$	0.274		0.272		0.262		0.371		0.369		0.376	
K_d	1.013		1.041		1.257		1.007		1.039		1.255	
$\theta_L \backslash \theta_T$	K_{bL}	K_{bT}	K_{bL}	K_{bT}	K_{bL}	K_{bT}	K_{bL}	K_{bT}	K_{bL}	K_{bT}	K_{bL}	K_{bT}
0	1,00	1,00	1,00	1,00	1.00	1.00	1,00	1,00	1,00	1,00	1.00	1.00
10	0,98	0,98	0,98	0,97	1.00	1.02	0,99	1,01	1,00	1,01	0.98	1.01
20	0,98	1,03	0,97	1,03	1.00	1.10	0,99	1,07	1,00	1,08	1.00	1.07
30	0,98	1,12	0,97	1,13	1.00	1.15	1,00	1,15	1,00	1,18	1.00	1.20
40	0,94	1,25	0,93	1,29	1.00	1.33	0,97	1,29	0,97	1,34	0.93	1.39
50	0,75	1,46	0,72	1,54	0.78	1.56	0,77	1,40	0,78	1,48	0.74	1.58
60	0,57	1,76	0,56	1,93	0.59	2.08	0,58	1,44	0,58	1,54	0.56	1.57
70	0,38	1,62	0,37	1,87	0.39	2.35	0,39	1,18	0,39	1,27	0.37	1.68
80	0,19	0,81	0,19	0,94	0.20	1.18	0,19	0,59	0,19	0,64	0.19	0.84
90	0	0	0	0	0	0	0	0	0	0	0	0

All these results are consistent with Eq. (14) and the inclusion of the diffuse fraction in the parameter conversion process. From this equation it can be seen that when the diffuse fraction is small $K_b = K_{hem}$; this happens for example at low angles of incidence. In contrast, when the diffuse fraction is larger (larger angles of incidence), the differences between K_b and K_{hem} are significant and the parameter conversion becomes more consistent with the results of the QDT method. The latter method includes the diffuse fraction in its thermal model.

5. Conclusions

The thermal performance test procedures for evacuated tube solar collectors with heat pipes have been analyzed using two different test methods: SST and QDT (ISO-9806, 2017). The experimental estimation of the IAM of the ETC-HP technology was improved by proposing modifications to both test methods, and two solar collectors of this type were considered to evaluate these modifications.

A novel IAM model for the QDT method was presented and validated against the SST results. This model was originally developed for flat plate collectors, and in this case its superiority over other models has already been demonstrated (Rodríguez-Muñoz et al., 2021b). This work further highlights the versatility of application of this model, as it is applicable to both uniaxial and biaxial IAM collectors. The versatility and superior performance of this model make it suitable for use as a general model in testing standards.

The role of the data averaging time in the QDT test was also analyzed, and variability in the results was observed. Based on the comparison with the SST test results, it was concluded that an averaging time of 10 minutes is the most suitable choice for this methodology. We recognize this variability as a drawback of the QDT method, and consequently, the improvement of this aspect represents an area for future research. As mentioned in the previous section, an alternative approach could involve the utilization of dynamic identification algorithms, which have demonstrated advantages in modeling the transient effects of various collector types (Spirkl et al., 1997; Hofer et al., 2015; Fahr et al., 2018; Rodríguez-Muñoz et al., 2021a).

Finally, to improve compatibility between testing methodologies, an alternative parameter conversion procedure from SST to QDT was proposed. The main differences between the testing methods were found in the incidence angle modifiers and the effective thermal capacity. The proposed method specifically addresses the incidence angle modifiers difference. It incorporates the diffuse fraction in the data processing of the IAM SST method, leading to improved results, especially for high angles of incidence where the diffuse radiation influence increase. The application of this method reduces the K_d differences between QDT and SST from 9 % and 45 % to differences between 8 % and 26 %, depending on the angle of incidence. Higher reductions are observed for larger incidence angles. Although this work introduces improved methods and analysis for setting parameters based on experimental evidence, it is important to note that this proposal only partially resolves the SST-QDT differences, and further research is necessary in this area.

Regarding future studies, in addition to the aforementioned differences regarding the IAM, significant disparities were observed in the estimation of the effective thermal capacity per unit area (a_5). The values obtained from both testing methods appear to be unusually high considering the physical composition of the collectors. Addressing and improving the determination of this parameter represents another area for future research, especially in the QDT method, where all parameters are determined simultaneously. Further studies are also needed, taking into account different collector types, to confirm the advantages of the proposed approach and to demonstrate its general applicability across different technologies.

Acknowledgments

The authors would like to thank the Ministerio de Industria, Energía y Minería (MIEM, Uruguay), especially its Dirección Nacional de Energía (DNE), the Fideicomiso Uruguayo de Ahorro y Eficiencia Energética (Fudaee, Uruguay) and the Corporación Nacional para el Desarrollo (CND, Uruguay), for having provided financial and logistical support for the development of the BECS facility and for having promoted this project with local capacities. The authors are also grateful to the PTB of Germany for promoting and financing the inter-laboratory on efficiency test of solar collectors, which has given us technical certainty about our local testing capabilities. The authors acknowledge partial financial support from CSIC Research Group Program, Universidad de la República, Uruguay.

Appendix A. Tests checks according to the ISO 9806:2017

Figure A.1 shows the graphs suggested by the standard to assess the variability of the operating conditions of the measurement set, where each data point (blue) corresponds to a 10 minute average. The data shown correspond to the ETC-HP-1 collector. The plots for ETC-HP-2 were omitted because they are very similar to those for ETC-HP-1 and do not provide any additional information. In Figure A.1a, clear sky and cloudy conditions can be distinguished, with clear sky values showing a more consistent pattern. The red line with a slope of 1 ($G_t = G_{dt}$) in this figure is used for basic quality control; the G_{dt} and G_t measurements should be below the red line, since $G_{dt} \leq G_t$. Figure A.1b shows the different inlet temperatures, while Figure A.1c shows the variability in the angle of incidence. Negative and positive values in the latter graph correspond to measurements taken before and after solar noon, respectively. Finally, Figure A.1d shows the variability of the wind speed parallel to the plane of the collector. Although certain wind speed values exceed the upper limit specified in the standard (as shown in Table 1), it is well known that the thermal performance of this type of collector (double cover with vacuum between them) is not significantly affected by wind speed (Zambolin & Del Col, 2012). Therefore, these occasional high wind speeds are not expected to have a significant impact on the results.

Appendix B. Data and software availability

To facilitate the reproduction of QDT tests for ETC collectors, a Matlab program is provided with the implementation of this algorithm, which can be downloaded here. Although initially developed for ETC collectors, the program has broader applicability and allows the identification of parameters for low-temperature collectors with uniaxial or biaxial IAM. The program employs a constrained nonlinear regression algorithm to calculate and report the values of the characteristic parameters, along with their typical uncertainties and t-statistics (the ratio between the parameter value and its uncertainty). For parameter a_2, it is possible to set the upper and lower limit arbitrarily, which allows setting the parameter to zero if a positive value is obtained with a t-statistic less than 3 (in this case, both limits must be set to zero). However, note that the program does not verify the quality of the experimental data set or compliance with the requirements of the ISO-9806 (2017) standard, which should be ensured prior to utilization. Nevertheless, it does provide the recommended graphs to assess the variability of the data set. The software is provided with the two experimental data sets used in this work.

References

ASHRAE-93 (2014). *Methods of Testing to Determine the Thermal Performance of Solar Collectorss*. Standard American Society of Heating, Refrigerating and Air-Conditioning Engineers USA.

Bates, D. M., & Watts, D. G. (1988). *Nonlinear regression analysis and its applications*. John Wiley & Sons.

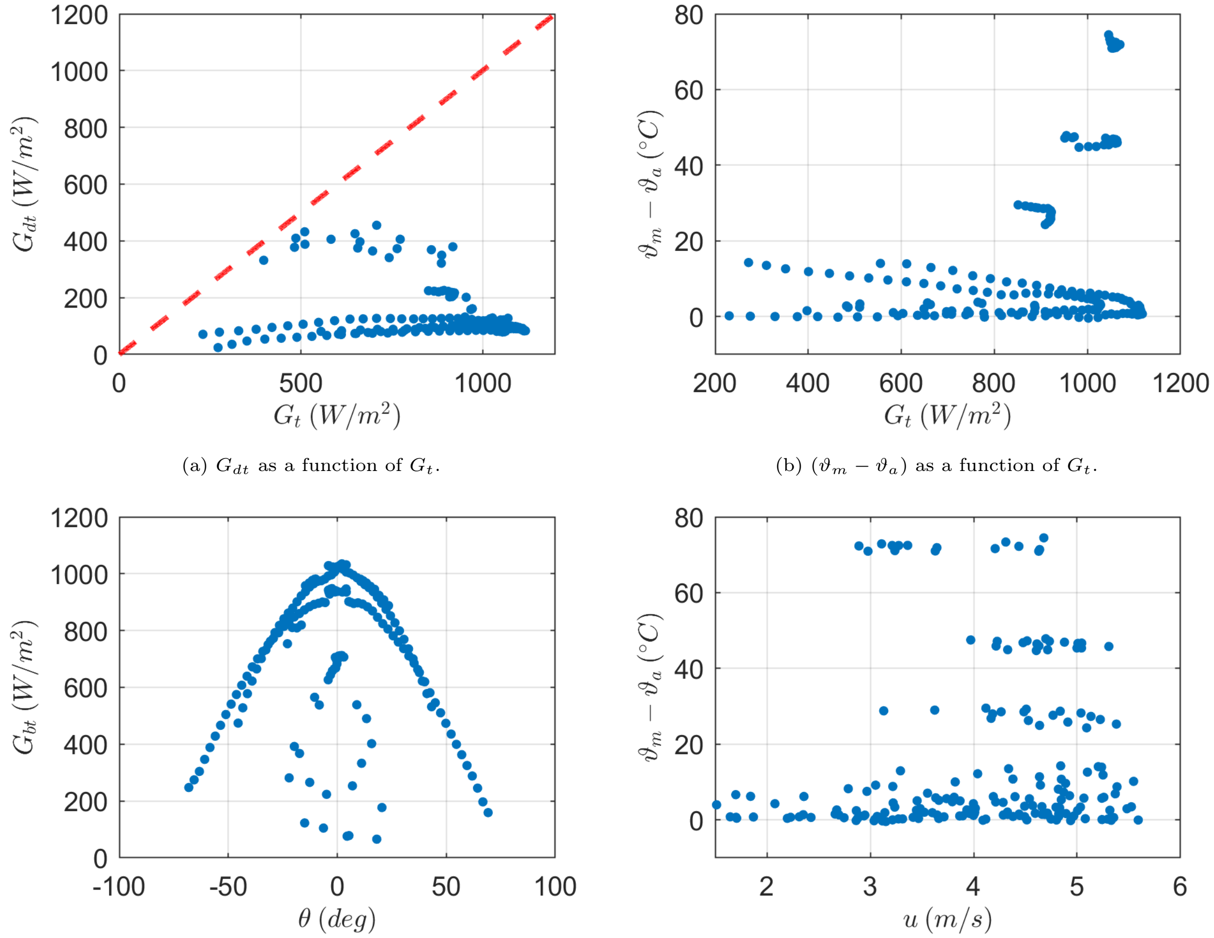

(a) G_{dt} as a function of G_t.

(b) $(\vartheta_m - \vartheta_a)$ as a function of G_t.

(c) G_{bt} as a function of θ.

(d) $(\vartheta_m - \vartheta_a)$ as function of u.

Figure A.1: Data set used for the parameter identification of the ETC-HP-1 collector, following the standard recommendations.

Bertsekas, D. (1999). *Nonlinear Programming*. Athena Scientific.

Brunger, A. P., & Hooper, F. C. (1993). Anisotropic sky radiance model based on narrow field of view measurements of shortwave radiance. *Solar Energy*, *51*, 53 – 64. doi:https://doi.org/10.1016/0038-092X(93)90042-M.

Duffie, J. A., & Beckman, W. A. (1991). *Solar engineering of thermal processes*. John Wiley & Sons.

EN-12975 (2022). *Solar collectors - General requirements*. Standard European Committee for Standardisation Belgium.

Fahr, S., Gumbel, U., Zirkel-Hofer, A., & Kramer, K. (2018). In situ characterization of thermal collectors in field installations. In *Proceedings of EuroSun*. doi:0.18086/eurosun2018.12.01.

Fischer, S. (2020). *Quality Infrastructure for Energy Efficiency and Renewable Energy in Latin America and the Caribbean, Report # 95309*. Report Intituto Metrológico Aleman - PTB.

Fischer, S., Heidemann, W., Müller-Steinhagen, H., Perers, B., Bergquist, P., & Hellström, B. (2004). Collector test method under quasi-dynamic conditions according to the european standard en 12975-2. *Solar Energy*, *76*, 117 – 123. doi:https://doi.org/10.1016/j.solener.2003.07.021.

Fischer, S., Lüpfert, E., & Müller-Steinhagen, H. (2006). Efficiency testing of parabolic trough collectors using the quasi-dynamic test procedure according to the european standard en 12975. In *SolarPACES 13th symposium on concentrating* *solar power and chemical energy technologies*.

Hofer, A., Büchner, D., Kramer, K., Fahr, S., Heimsath, A., Platzer, W., & Scholl, S. (2015). Comparison of two different (quasi-) dynamic testing methods for the performance evaluation of a linear fresnel process heat collector. *Energy Procedia*, *69*, 84–95. doi:https://doi.org/10.1016/j.egypro.2015.03.011. International Conference on Concentrating Solar Power and Chemical Energy Systems, SolarPACES 2014.

ISO-9488 (2022). *Solar energy — Vocabulary*. Standard International Organization of Standarization Switzerland.

ISO-9806 (2017). *Solar Energy – Solar thermal collectors – Test methods*. Standard International Organization of Standarization Switzerland.

García de Jalón, A., Sallaberry, F., Olano, X., , Mateu, E., Astiz, R., Ezcurra, M., & Ramíres, L. (2011). Comprarison of thermal efficiency curves of solar collectors tested in outdoor conditions. In *Proceedings of ISES World Congress 2011*.

Janotte, N., Meiser, S., Krüger, D., Lüpfert, E., Pitz-Paal, R., Fischer, S., & Müller-Steinhagen, H. (2009). Quasi-dynamic analysis of thermal performance of parabolic trough collectors. In *SolarPACES 2009 Conference Proceedings*.

Kalogirou, S. A. (2004). Solar thermal collectors and applications. *Progress in Energy and Combustion Science*, *30*, 231 – 295. doi:https://doi.org/10.1016/j.pecs.2004.02.001.

Kong, W., Perers, B., Fan, J., Furbo, S., & Bava, F. (2015). A new laplace transformation method for dynamic testing of solar collectors. *Renewable Energy*, *75*, 448–458. URL: https://www.sciencedirect.com/science/article/pii/S0960148114006533. doi:https://doi.org/10.1016/j.renene.2014.10.026.

Kong, W., Wang, Z., Fan, J., Bacher, P., Perers, B., Chen, Z., & Furbo, S. (2012). An improved dynamic test method for solar collectors. *Solar Energy*, *86*, 1838 – 1848. doi:https://doi.org/10.1016/j.solener.2012.03.002.

Kovács, P., Pettersson, U., Persson, M., Perers, B., & Fischer, S. (2011). Improving the accurancy in performance prediction for new collector desings. In *Proceedings of Solar World Congress*.

Kratzenberg, M., Beyer, H., & Colle, S. (2006). Uncertainty calculation applied to different regression methods in the quasi-dynamic collector test. *Solar Energy*, *80*, 1453 – 1462. doi:https://doi.org/10.1016/j.solener.2006.03.010.

Kumar, A., Said, Z., & Bellos, E. (2021). An up-to-date review on evacuated tube solar collectors. *Journal of Thermal Analysis and Calorimetry*, *145*, 2873–2889.

McIntire, W. R. (1982). Factored approximations for biaxial incident angle modifiers. *Solar Energy*, *29*, 315 – 322. doi:https://doi.org/10.1016/0038-092X(82)90246-8.

Osório, T., & Carvalho, M. J. (2014). Testing of solar thermal collectors under transient conditions. *Solar Energy*, *104*, 71 – 81. doi:https://doi.org/10.1016/j.solener.2014.01.048. Solar heating and cooling.

Perers, B. (1997). An improved dynamic solar collector test method for determination of non-linear optical and thermal characteristics with multiple regression. *Solar Energy*, *59*, 163 – 178. doi:https://doi.org/10.1016/S0038-092X(97)00147-3.

QAiST (2012). *Performance testing of evacuated tubular collectors*. Report Quality Assurance in Solar heating and cooling Technology.

Rodríguez-Muñoz, J. M. (2021). *Ensayos de desempeño térmico de colectores solares de placa plana*. Thesis Universidad de la República (Uruguay). Facultad de Ingeniería. doi:10.13140/RG.2.2.23050.18881.

Rodríguez-Muñoz, J. M., Bove, I., & Alonso-Suárez., R. (2021a). A detailed dynamic parameter identification procedure for quasi-dynamic testing of solar thermal collectors. In *Proceedings of Solar World Congress*. doi:doi:10.18086/swc.2021.25.01.

Rodríguez-Muñoz, J. M., Bove, I., & Alonso-Suárez, R. (2021b). Novel incident angle modifier model for quasi-dynamic testing of flat plate solar thermal collectors. *Solar Energy*, *224*, 112–124. doi:https://doi.org/10.1016/j.solener.2021.05.026.

Rodríguez-Muñoz, J. M., Monetta, A., Alonso-Suárez, R., Bove, I., & Abal, G. (2021c). Correction methods for shadow-band diffuse irradiance measurements: assessing the impact of local adaptation. *Renewable Energy*, *178*, 830–844. doi:https://doi.org/10.1016/j.renene.2021.06.102.

Rodríguez-Muñoz, J. M., Monetta, A., Bove, I., & Alonso-Suárez, R. (2020). Ensayo cuasi-dinámico de colectores solares de placa plana en uruguay de acuerdo a la norma iso 9806:2017. *ENERLAC. Revista de energía de Latinoamérica y el Caribe*, *4*, 10–26.

Rojas, D., Beermann, J., Klein, S., & Reindl, D. (2008). Thermal performance testing of flat-plate collectors. *Solar Energy*, *82*, 746 – 757. doi:https://doi.org/10.1016/j.solener.2008.02.001.

Sallaberry, F., García de Jalón, A., Olano, X., Mateu, E., Erice, R., & Ramirez, L. (2011). Bi-axial incidence angle modifier using quasi-dynamic test for asymmetrical solar collector using dummy variables. In *ESTEC congress, Marseille (France)*.

Souka, A., & Safwat, H. (1966). Determination of the optimum orientations for the double-exposure, flat-plate collector and its reflectors. *Solar Energy*, *10*, 170 – 174. doi:https://doi.org/10.1016/0038-092X(66)90004-1.

Spirkl, W., Muschaweck, J., Kronthaler, P., Scholkopf, W., & Spehr, J. (1997). In situ characterization of solar flat plate collectors under intermittent operation. *Solar Energy*, *61*, 147–152.

Theunissen, P.-H., & Beckman, W. (1985). Solar transmittance characteristics of evacuated tubular collectors with diffuse back reflectors. *Solar Energy*, *35*, 311–320. doi:https://doi.org/10.1016/0038-092X(85)90139-2.

Xu, L., Wang, Z., Li, X., Yuan, G., Sun, F., & Lei, D. (2013). Dynamic test model for the transient thermal performance of parabolic trough solar collectors. *Solar Energy*, *95*, 65–78. URL: https://www.sciencedirect.com/science/article/pii/S0038092X13002089. doi:https://doi.org/10.1016/j.solener.2013.05.017.

Xu, L., Wang, Z., Yuan, G., Li, X., & Ruan, Y. (2012). A new dynamic test method for thermal performance of all-glass evacuated solar air collectors. *Solar Energy*, *86*, 1222–1231. URL: https://www.sciencedirect.com/science/article/pii/S0038092X1200031X. doi:https://doi.org/10.1016/j.solener.2012.01.015.

Zambolin, E., & Del Col, D. (2012). An improved procedure for the experimental characterization of optical efficiency in evacuated tube solar collectors. *Renewable Energy*, *43*, 37 – 46. doi:https://doi.org/10.1016/j.renene.2011.11.011.